Available online at www.sciencedirect.com
ScienceDirect
Energy Conversion and Management 48 (2007) 2775–2783
ENERGY CONVERSION & MANAGEMENT
www.elsevier.com/locate/enconman

# Direct numerical simulation of a heat removal configuration for fusion blankets

S.C. Kakarantzas [a], A.P. Grecos [a], N.S. Vlachos [a,*], I.E. Sarris [b], B. Knaepen [b], D. Carati [b]

[a] Department of Mechanical and Industrial Engineering, University of Thessaly, Athens Avenue, 38334 Volos, Greece
[b] Université Libre de Bruxelles, Physique Statistique et Plasmas, CP 231, Campus Plaine, 1050 Brussels, Belgium

Available online 11 September 2007

**Abstract**

A series of direct numerical simulations (DNS) are performed to study the natural convection heat transfer between concentric cylinders at several Rayleigh and Hartmann numbers. The buoyant flow is driven by the temperature difference between the inner and the outer walls, with the inner wall being at lower temperature, while an external transverse magnetic field is imposed. Both laminar and turbulent flows are observed depending on the magnitude of the Rayleigh and Hartmann numbers. The resulting flow structures of the cases studied were both laminar and turbulent. The results show the 3D nature of turbulence and the tendency of the magnetic field to form narrow Hartmann layers, 3D jets and wakes at specific azimuthal angles. Some particular features of the turbulent regime as well as the heat transfer are also investigated. The magnetic field effect on the convective heat transfer is assessed via the Nusselt number showing that conduction dominates as the Hartmann number increases.


*Keywords:* Natural convection; Magnetohydrodynamics; Direct numerical simulation; Heat removal; Fusion blankets

## 1. Introduction

In the last decades, numerous studies have dealt with magnetohydrodynamic (MHD) liquid metal flow and heat transfer. The basic motivation has been the efficient design of the blanket of the magnetically confined fusion reactor. The main research efforts in such configurations relate to increasing the heat transfer and decreasing the fluid pressure drop along the flow channel. The pressure drop in MHD pipes and ducts is proportional to the Hartmann number, implying that the stronger the magnetic field, the more expensive the fluid pumping for heat removal. Thus, avoiding heat removal by forced convection and using efficient natural convection as an alternative, it may be more economic. Because a significant amount of heat in the blanket is due to nuclear irradiation, the best choice for the working fluid is liquid metal, but the presence of strong magnetic fields may suppress the fluid motion and reduce the required heat transfer rates [1]. An alternative configuration proposed recently [2,3] (consisting of two concentric cylinders, where the liquid metal is placed between the cylinders and a non-conductive gas in the internal cylinder) may reduce significantly the negative MHD effects. By using this configuration, the non-conductive gas can remove the heat without any additional pressure drop due to the presence of the magnetic field. This constant-in-time process of heat removal keeps the inner cylinder in lower temperature than the external one.

Among the relevant MHD investigations, Uda et al. [4] studied both experimentally and numerically a natural convection liquid metal flow between a tube and a heater pin that was placed on the axis of the tube. A transverse magnetic field was applied on the fluid and the mechanism of heat transfer was studied. For their simulations the $k-\epsilon$ model as adapted for MHD natural convection flows model has been used. Moreover, Serizawa et al. [3] performed an experiment in a vertical tube using a NaK/Nitrogen flow and applying an external transverse

* Corresponding author. Tel.: +30 24210 74094; fax: +30 24210 74085.
*E-mail addresses:* vlachos@mie.uth.gr (N.S. Vlachos), sarris@mie.uth.gr (I.E. Sarris).

0196-8904/$ - see front matter © 2007 Elsevier Ltd. All rights reserved.
doi:10.1016/j.enconman.2007.07.024

**Nomenclature**

| | |
|---|---|
| $B_0$ | magnitude of the external magnetic field (kg/(s$^2$ A)) |
| $H$ | aspect ratio $H = L/R = 3$ |
| $p$ | fluid pressure (bar) |
| $L$ | length of the cylinders (m) |
| $u_z$, $u_r$, $u_\theta$ | non-dimensional axial, radial, circumferential velocity components |
| $R = R_o - R_i$ | the gap between the cylinders (m) |
| $R_o$ | radius of the outer cylinder (m) |
| $R_i$ | radius of the inner cylinder (m) |
| $r_o$ | non-dimensional radius of the outer cylinder |
| $r_i$ | non-dimensional radius of the inner cylinder |
| $Nu$ | Nusselt number |
| $T_o$ | temperature of the outer wall (K) |
| $T_i$ | temperature of the inner wall (K) |
| $r$, $\theta$, $z$ | spatial coordinates |
| $\Delta T = T_o - T_i$ | temperature difference between the cylinders (K) |
| $Pr = \nu/\alpha$ | Prandtl number |
| $Ra = g\beta\Delta TR^3/\nu\alpha$ | Rayleigh number |
| $Ha = \sqrt{\sigma/\rho\nu}B_0R$ | Hartmann number |
| $t$ | time (s) |
| $\Delta t$ | time step (s) |
| $g$ | gravity acceleration (m/s$^2$) |
| *Greek letters* | |
| $\nu$ | fluid kinematic viscosity (m$^2$/s) |
| $\rho$ | fluid density (kg/m$^3$) |
| $\sigma$ | electric conductivity (ms$^3$ A$^2$/kg) |
| $\Phi$ | electric potential (m$^2$ kg/s$^3$ A) |
| $\tau$ | non-dimensional time |
| $\alpha$ | thermal diffusivity (m$^2$/s) |
| $\beta$ | coefficient of thermal expansion (1/K) |
| $\Psi$ | non-dimensional stream function |

magnetic field, demonstrating that the heat transfer was asymmetric. Similar results were found in the numerical study of Li et al. [2] for a liquid metal/gas annular flow in a vertical pipe under the effect of a transverse magnetic field.

In the present work a similar configuration is considered where a liquid metal is placed between two coaxial vertical cylinders while an external transverse magnetic field is applied. The main purpose is to investigate the basic hydrodynamic natural convection flow and the effect of the magnetic field on the MHD flow and heat transfer. In difference to previous studies, the effect of the magnetic field on the 3D turbulent heat transfer regime is investigated. This regime corresponds to certain combination of the flow controlling parameters such as the Rayleigh and Hartmann numbers.

## 2. Problem description and model setup

A closed concentric cylindrical configuration shown in Fig. 1 is used with an aspect ratio $H = L/R = 3$, where $L$ is the length of the cylinders, and the annular gap $R = R_o - R_i$ where $R_o$, $R_i$ are the radius of the outer and inner cylinders, respectively. The non-dimensional radius of the cylinders are $r_i = R_i/R = 0.2$ and $r_o = R_o/R = 1.2$. While preliminary simulations were done using an aspect ratio of 1, it was decided to concentrate on more elongated domains mainly because they are more representative of the one that may be used in the liquid metal blankets. The choice of aspect ratio 3 corresponds to a fair balance between the actual design needs of the blankets and the efficiency of the used direct numerical simulation method. Both outer and inner walls are assumed isothermal, with the outer wall temperature $T_o$ greater than that of the inner wall $T_i$. A liquid metal with Prandtl number of 0.0321 is placed between the cylinders, interacting with an external transverse magnetic field $B_0$. Any flow-induced magnetic field is assumed to be very small in comparison to the external field and, thus, the low magnetic Reynolds number approximation is adopted [5].

The magnetohydrodynamic equations (continuity, Navier–Stokes, energy and electric potential) were made dimensionless using as characteristic quantities, the distance $R$ between the two cylinders, the temperature difference $\Delta T = T_o - T_i$, the free fall velocity $u_{ref} = \sqrt{g\beta\Delta TR}$, the magnitude of the external magnetic field $B_0$, an electrical potential $Ru_{ref}B_0$ and a reference time $R/u_{ref}$:

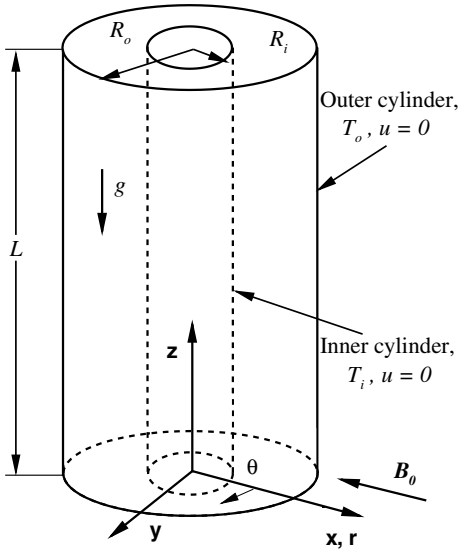


Fig. 1. Flow configuration and boundary conditions.

$$\nabla \cdot \boldsymbol{v} = 0, \tag{1}$$

$$\frac{\partial \boldsymbol{v}}{\partial t} + (\boldsymbol{v}\cdot\nabla)\boldsymbol{v} = -\nabla p + T_z + \left(\frac{Pr}{Ra}\right)^{\frac{1}{2}}\nabla^2\boldsymbol{v} + Ha^2\left(\frac{Pr}{Ra}\right)^{\frac{1}{2}}(\boldsymbol{J}\times\boldsymbol{B}_0), \tag{2}$$

$$\frac{\partial T}{\partial t} + (\boldsymbol{v}\cdot\nabla)T = \left(\frac{1}{PrRa}\right)^{\frac{1}{2}}\nabla^2 T, \tag{3}$$

$$\nabla^2\Phi = \nabla\cdot(\boldsymbol{v}\times\boldsymbol{B}_0), \tag{4}$$

$$\boldsymbol{J} = -\nabla\Phi + \boldsymbol{v}\times\boldsymbol{B}_0, \tag{5}$$

where $T = (T^* - T_i)/(T_o - T_i)$ is the dimensionless temperature, $p$ is the pressure, and $\boldsymbol{J}$, $\Phi$ are the electric current and electrical potential, respectively.

The liquid metal is considered as Newtonian, the Boussinesq approximation is used for the buoyancy term, and the effects of viscous dissipation and Joule heating are neglected. These simplifications are almost universal for all MHD natural convection flows. The Rayleigh number is defined as $Ra = g\beta\Delta TR^3/\nu\alpha$, the Hartmann number as $Ha = \sqrt{\sigma/\rho\nu}B_0R$, and the Prandtl number as $Pr = \nu/\alpha$. No slip conditions are assumed on the walls ($u_r = u_\theta = u_z = 0$ for $z = 0$ and $H$, $r = r_i$ and $r_o$), constant temperatures at the inner and outer cylindrical walls ($T = 0$ for $r = r_i$, $T = 1$ for $r = r_o$), and zero heat fluxes at the bottom and top walls (i.e., adiabatic conditions $\frac{\partial T}{\partial z} = 0$ for $z = 0$, $H$). Also the normal derivative of the electrical potential is kept zero at the walls: $\partial\Phi/\partial n = 0$.

Heat transfer is assessed via the local and average Nusselt numbers. The local Nusselt numbers along the inner and outer cylinders are calculated as the actual heat transfer divided by the heat conduction

$$Nu_i(\theta) = \ln\left(\frac{r_i}{r_o}\right)\left(r\frac{\partial T}{\partial r}\right)_{r=r_i},$$
$$Nu_o(\theta) = \ln\left(\frac{r_i}{r_o}\right)\left(r\frac{\partial T}{\partial r}\right)_{r=r_o}. \tag{6}$$

The azimuthally averaged Nusselt numbers at the inner and outer cylinders are given by

$$\overline{Nu}_i = \frac{1}{2\pi}\int_0^{2\pi} Nu_i(\theta)\,d\theta, \quad \overline{Nu}_o = \frac{1}{2\pi}\int_0^{2\pi} Nu_o(\theta)\,d\theta, \tag{7}$$

while the total averaged (i.e., axially and azimuthally) Nusselt numbers at the inner and outer surfaces are calculated, as

$$\overline{Nu}_{i,tot} = \frac{1}{2\pi L}\int_0^{2\pi}\int_0^{L} Nu_i(\theta)\,dz\,d\theta,$$
$$\overline{Nu}_{o,tot} = \frac{1}{2\pi L}\int_0^{2\pi}\int_0^{L} Nu_o(\theta)\,dz\,d\theta. \tag{8}$$

In the present study, direct numerical simulations were conducted for two $Ra$ values (one corresponding to laminar and the other to turbulent flow) and for various values of $Ha$. The use of DNS instead of Reynolds-averaged models for the present flow was preferred because it gives the finest description of the flow and heat transfer phenomena while it was feasible with the available computer facilities for the range of parameters used. Furthermore, the increase of $Ha$ may cause transition of the turbulent flow to laminar that is very difficult to be studied with Reynolds-averaged models. The governing equations were discretized in a staggered non-uniform mesh with second-order accurate finite difference schemes [6]. The resulting system of algebraic equations was solved with a fractional step method where a hybrid scheme was used for the time integration. The diffusion terms were advanced in time with a Crank–Nicolson method, while the non-linear terms, the buoyancy and Lorentz force terms with an economic third-order Runge–Kutta method [7]. The numerical model was verified using the numerical results of De Vahl Davis and Thomas [8] for a similar configuration but with the internal cylinder being hotter. The results presented in Fig. 2 show that the most grid-sensitive quantity, i.e., $Nu$, is very close predicted by the present numerical model.

For a resolved DNS, the specific features of the flow and heat transfer must be considered. In particular, the increase of $Ha$ results to smaller Hartmann layers of thickness $\sim 1/Ha$, while the increase of $Ra$ results to smaller Kolmogorov scales, boundary layers and Batchelor scales. All these requirements were taken into account in the present direct numerical simulations by using the analysis proposed by Grötzbach [9] where the appropriate Kolmogorov scale $\eta$ can be a function of $Nu$ for fluids with $Pr < 1$. The value of $Nu$ needed for the grid sizing is given by an exponential function of $Ra$ and $Ha$ for MHD natural convection flows according to Aurnou and Olson [10]. As a result, two non-uniform grids of $32\times32\times96$ and $64\times64\times128$ (azimuthal, radial and axial directions) were used for the simulation of two cases with $Ra = 10^3$ and $10^5$, respectively. The assumption for the construction of the grid was tested by performing also a grid independence test. For this purpose, the more demanding MHD case of $Ra = 10^5$ and $Ha = 100$ was chosen. The range of the grids used in these tests and the results of each case are presented in Table 1. The comparison of the different quantities (maximum or minimum values of all velocity components or the Nusselt number that is the most sensitive to the grid size) justifies the

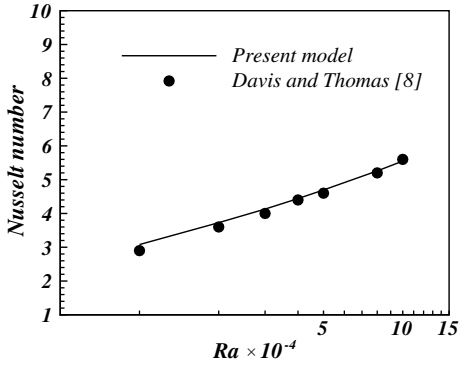


Fig. 2. Comparison of predicted $Nu$ with the results of De Vahl Davis and Thomas [8].

Table 1
Grid independence test for the case $Ra = 10^5$ and $Ha = 100$

| Grid | $32 \times 32 \times 64$ | $64 \times 64 \times 128$ | $97 \times 97 \times 176$ | $181 \times 181 \times 353$ |
|---|---|---|---|---|
| $u_{\theta,\max}$ | 0.225 | 0.381 | 0.404 | 0.394 |
| $u_{\theta,\min}$ | −0.337 | −0.457 | −0.456 | −0.410 |
| $u_{r,\max}$ | 0.342 | 0.292 | 0.294 | 0.340 |
| $u_{r,\min}$ | −0.336 | −0.468 | −0.498 | −0.450 |
| $u_{z,\max}$ | 0.430 | 0.741 | 0.754 | 0.787 |
| $u_{z,\max}$ | −0.604 | −0.756 | −0.731 | −0.820 |
| $Nu$ | 1.843 | 2.126 | 2.159 | 2.182 |

choice of the used grid, as well as the methodology used for its determination.

The range of the $Ra$ numbers considered here can be found in the specific conceptual design of the fusion blanket system, although higher $Ra$ values can also be observed. Moreover, although the selected maximum $Ha$ number of 100 laminarizes the flow, even much higher values of $Ha$ are expected in the real blanket. Thus, the use of fine grids at the Hartmann layers and the transitional regime of the MHD flow as the magnetic field increases may render the DNS an unavoidable tool for accurate simulations.

## 3. Results and discussion

The hydrodynamic simulations (i.e., $Ha = 0$) for each Ra were started using arbitrary flow and thermal fields and the time integration stopped when stationary or steady state flow was reached. The simulations for nonzero $Ha$ values were restarted using the hydrodynamic cases as initial conditions.

### 3.1. Laminar flow case – $Ra = 10^3$

For the laminar flow case ($Ra = 10^3$) the effect of the magnetic field is illustrated in Fig. 3a–c where the axial velocity distribution is shown for $Ha = 0$, 25 and 100, respectively. As shown in Fig. 3a, when there is no magnetic field, a uniform axial velocity distribution is observed in the $\theta$ direction and as a result the flow is axisymmetric. The red color indicates the regions where the fluid ascends and the blue color those where it descends. When the magnetic field is imposed, the flow is characterized by interesting changes, mainly with respect to its axisymmetry, as it can be seen in the vector plots of Fig. 4 taken in two different $\theta = 0°$ and $\theta = 90°$ planes. As shown in Fig. 3b, two pairs of wakes are formed in the regions of the cylindrical walls parallel to the magnetic field and, as a result, the flow loses its axisymmetry. The usual action of an externally imposed uniform magnetic field on the flow of liquid metals is to form quasi-2D vortices aligned with the direction of the magnetic field. In these vortices, already studied for the case of Rayleigh–Bernard MHD convection [11], the fluid rotates in planes perpendicular to the magnetic field direction. The same phenomenon can also be observed in other wall-bounded flows, as the one studied here, forming vortices with 3D rather than quasi-2D patterns. This phenomenon, observed also for the concentric pipe flow studied by Todd [12], is more intense as the magnetic field increases (Fig. 3c). In this case the wakes are thinner and closer to the cylindrical walls parallel to the magnetic field. Consequently, when a magnetic field is applied, the flow should be treated as fully 3D, even in the laminar case.

The effect of the magnetic field on the temperature distribution is demonstrated in Fig. 5a–d, where the isotherms at $\theta = 0°$ are shown for $Ha = 0$, 10, 25 and 50, respectively. In the absence of a magnetic field (Fig. 5a) the curving of the isotherms near the bottom part of the annular cavity indicates that convection is the main heat transfer mechanism. The effect of the magnetic field is to decrease the heat convection as indicated by the smaller curvature of the isotherms in Fig. 5b, and for stronger magnetic fields heat conduction dominates as shown in Fig. 5c and d.

Fig. 6a and b shows the evolution of the velocity and Fig. 6c and d the evolution of the temperature at two axial positions ($z = 0.5$ and 1.7), at azimuthal angles $\theta = 0°$ and 90°, respectively, radial distance $r = 1.16$, and for $Ha = 0$, 25 and 50. The selected monitoring points are near the mid $z$-plane ($z = 1.7$) and the bottom ($z = 0.5$) of the flow domain. The solid lines correspond to the hydrodynamic case, and the other lines to different values of $Ha$ as indicated. The MHD cases were simulated starting from the same initial hydrodynamic fields (at time $t = 10$). The presence of the magnetic field produces 3D effects on the velocity field as shown in the velocity evolution. It should be

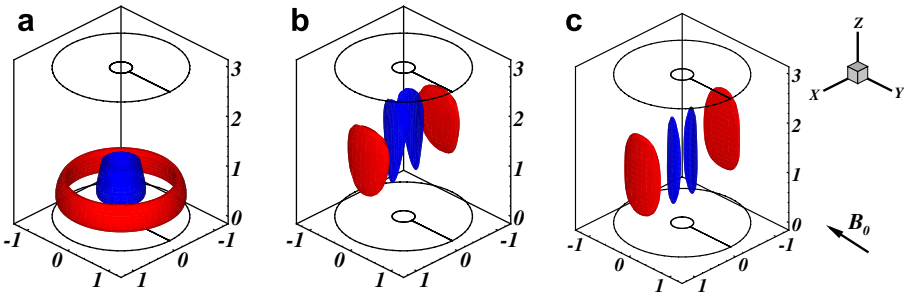


Fig. 3. Regions of ascending (red) and descending (blue) fluid for $Ra = 10^3$: (a) $Ha = 0$, (b) $Ha = 25$ and (c) $Ha = 100$. The axial velocity contour levels are: −1, 0.7 for $Ha = 0$, −0.4, 0.4 for $Ha = 25$ and −0.08, 0.1 for $Ha = 100$. (For interpretation of the references to color in this figure legend, the reader is referred to the web version of this article.)

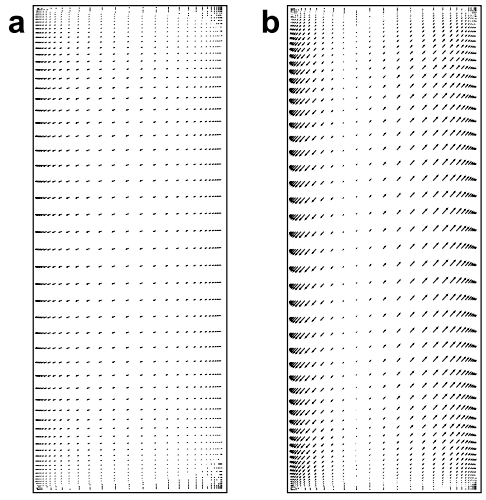


Fig. 4. Vector plots at planes (a) $\theta = 0°$ and (b) $\theta = 90°$ for $Ra = 10^3$ and $Ha = 50$.

noted that the temperature field remains almost axisymmetric for $Ha = 50$. It was found that the increase of $Ha$ leads to a decrease of total averaged Nusselt number at both surfaces (not shown here) and conduction becomes the main heat transfer mechanism.

### 3.2. Turbulent flow case – $Ra = 10^5$

The turbulent regime of this flow is also studied for $Ra = 10^5$ and several $Ha$ values. Although this Rayleigh number is not particularly high, after some initial transients, the resulting hydrodynamic flow sustained a stationary level of turbulence, as illustrated in Fig. 7a and b, where the instantaneous temperature and azimuthal velocity fields are shown, respectively. The breaking of the axisymmetry of the temperature field, as indicated by the isotherm $T = 0.75$ in Fig. 7a, is one of the main features of this turbulent flow, not present in the laminar case. The breaking of the temperature symmetry and the ensuing turbulent flow has as an immediate result the increase of the azimuthal velocity (Fig. 7b), producing fully 3D flow effects.

The complete turbulent behavior is depicted in Fig. 8a where the time evolution of the total kinetic and thermal energies of the flow is shown for $Ha = 0$, 50 and 100. The MHD cases were simulated starting from the same initial hydrodynamic fields (at time $t = 40$). The increase of $Ha$ results in the decrease of both these energies. For stronger magnetic fields ($Ha = 100$) the value of the kinetic energy becomes very small, as shown in Fig. 8a, indicating that the fluid motion has decreased significantly. The time evolution of both energies remains unchanged for the higher $Ha$ studied here, suggesting that the flow becomes steady state after a short time. This effect is also very well depicted in the temperature evolution at two internal locations of the flow, as shown in Fig. 8b. Both monitoring points are close to the bottom of the domain and close to the sidewalls. The increase of $Ha$ suppresses the temperature fluctuations. For the higher $Ha$ value studied, the resulting temperature value of the monitoring point near the external cylinder is very close to the values expected when heat conduction is the main transfer mechanism, i.e., when fluid velocity goes to zero. This result indicates that the primary effect of the magnetic field is to decrease convection heat transfer. The domination of conduction over convection heat transfer starts from the external cylinder rather than the internal one.

Before presenting the specific characteristics of the MHD flow, it will be interesting to describe the turbulent features of the hydrodynamic case shown in Fig. 9, where the instantaneous fields of some important turbulent quantities averaged over $\theta$ are presented. From left to right, these quantities are the isotherms, the average streamlines, the turbulent kinetic and thermal energies, azimuthal vorticity ($\omega_z$) and the Reynolds stresses $\overline{u'_\theta u'_\theta}$, $\overline{u'_r u'_r}$ and $\overline{u'_z u'_z}$.

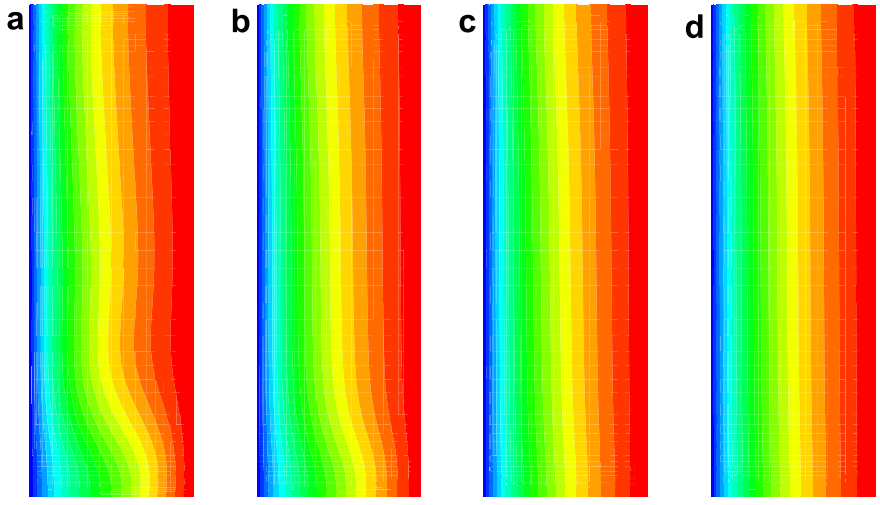


Fig. 5. Isotherms at $\theta = 0°$ for $Ra = 10^3$: (a) $Ha = 0$, (b) $Ha = 10$, (c) $Ha = 25$ and (d) $Ha = 50$.

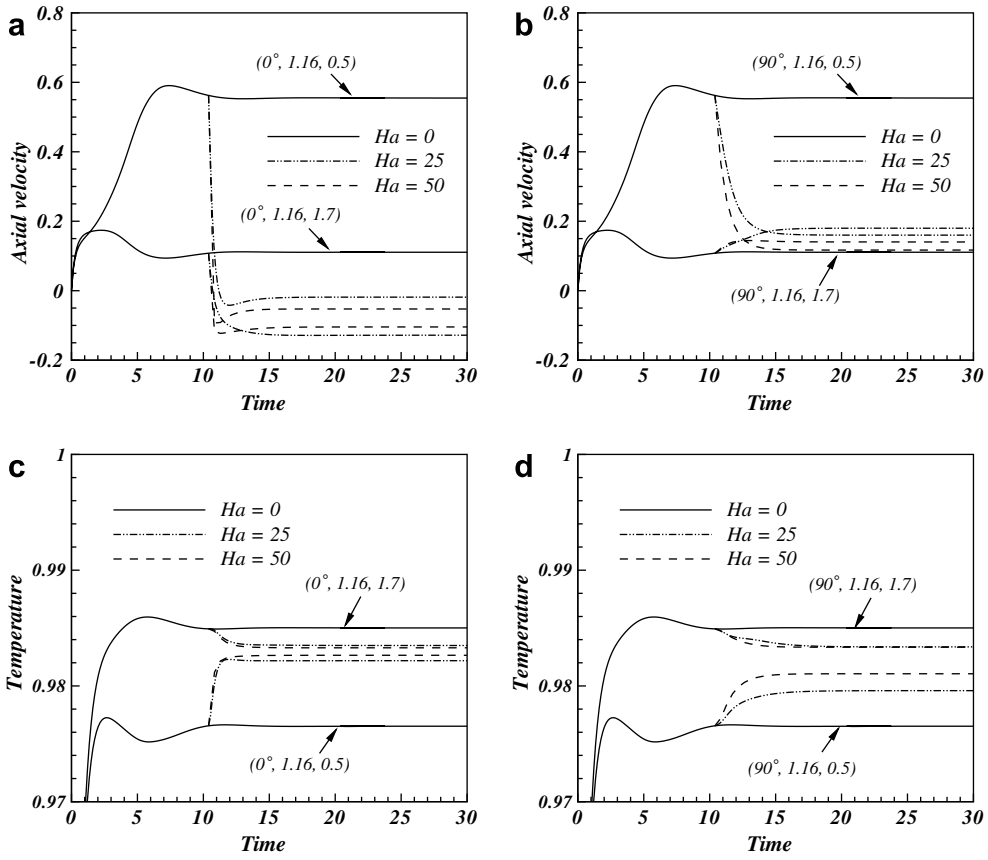


Fig. 6. Time evolution of axial velocity (top) and temperature (bottom) at $\theta = 0°$ (left) and $\theta = 90°$ (right), at positions $z = 0.5$ and 1.7, $r = 1.16$ and for $Ha = 0$, 25 and 50.

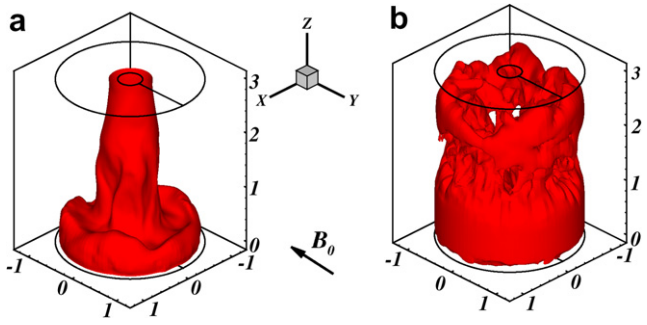


Fig. 7. Instantaneous temperature (a) and azimuthal velocity field (b) for $Ra = 10^5$ and $Ha = 0$.

The instantaneous flow is ascending across the hotter external cylinder and descending across the internal one. Except of the main flow patterns, several smaller circulation patterns are observed in the corners and near the surface of the external cylinder. The $\theta$-averaged fields of temperature $T$ and stream function are quite smooth as a result of the averaging over $\theta$. For the specific time of the snapshot, the highly unstable area of the flow field is in the corner formed by the internal cylinder with the bottom wall. In this region, the colder flow stream generates a counter-rotating vortex resulting in local enhancement of the turbulent kinetic energy, and consequently of the Reynolds stresses. Above this region, there is another one where instabilities are produced, mainly because of the local maximum of the thermal turbulent energy. Thus, both kinetic and thermal energies may be equally responsible for sustaining the turbulent fluctuations.

Almost the same turbulent features, as in the hydrodynamic case above, is observed for the MHD case of the low $Ha = 10$. However, for high $Ha$ values, an almost laminar flow occurs but with stronger convection currents than in the laminar case presented in Section 3.1. Fig. 10 illustrates the most important features of the MHD flow for $Ha = 100$ at time $t = 102$. Starting clockwise from the upper-left, the 3D distributions of the isotherms, axial velocity $u_z$, electric current $J_r$, and electric potential $\Phi$ are presented. The significant result of Fig. 10 is the strong connection between the electric, velocity and thermal fields. The non-uniformity of the temperature near the internal and external walls in the four regions where these walls are parallel to the magnetic field follows the pattern of the electric field, which is also observed in the velocity field. Thus, the fluid jets that are formed in these four regions are a direct effect of the magnetic field. Similar conclusions were also drawn by Todd [12] for the Hartmann flow in annular pipes.

Another important observation is the narrow Hartmann layers (at 90° and 270°) of the wakes near the

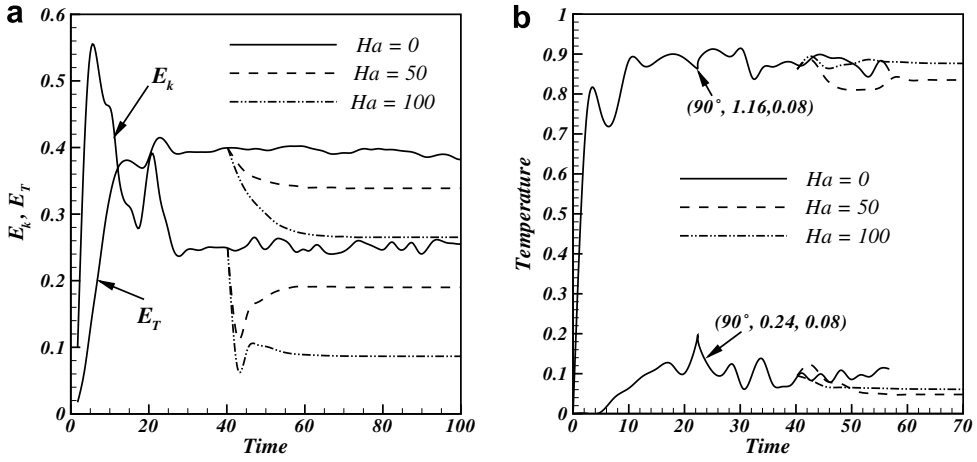


Fig. 8. Time evolution of (a) total kinetic and thermal energies and (b) temperature, for $Ra = 10^5$ at positions $r = 0.24$ and 1.16, $\theta = 90°$ and $z = 0.08$.

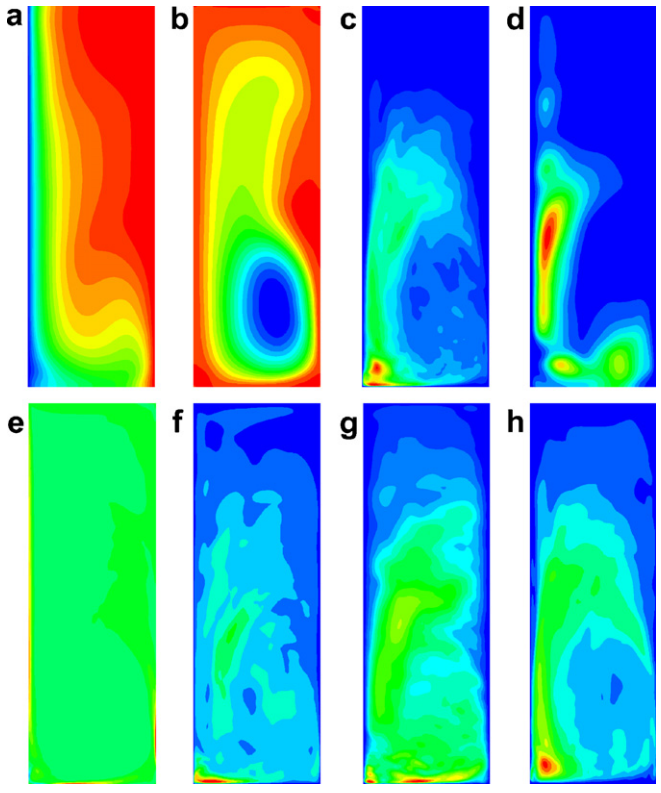


Fig. 9. Instantaneous turbulent quantities averaged over $\theta$ for $Ra = 10^5$ and $Ha = 0$. From left to right: isotherms, streamlines, turbulent kinetic and thermal energies, vorticity ($\omega_z$), and Reynolds stresses $\overline{u'_\theta u'_\theta}$, $\overline{u'_r u'_r}$, $\overline{u'_z u'_z}$.

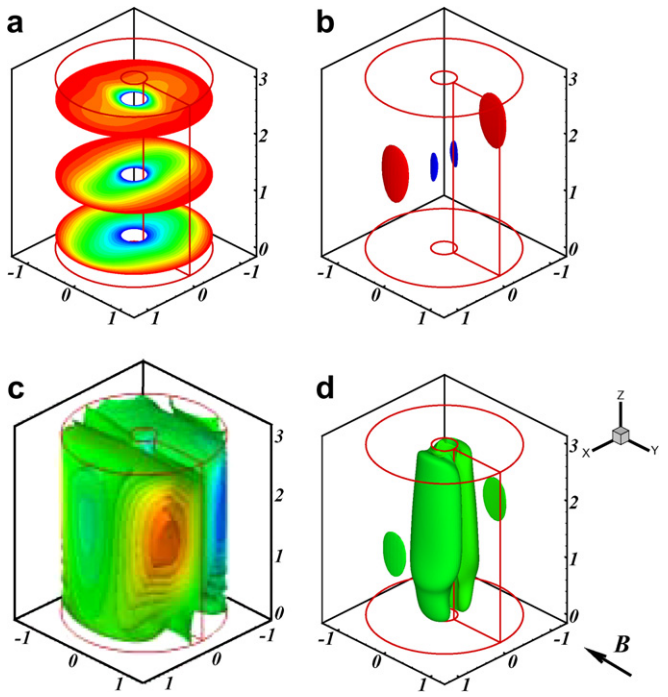


Fig. 10. 3D distribution of isotherms (upper-left), vertical velocity $u_z$ (upper right), electric potential $\Phi$ (lower left) and electric current $J_r$ (lower right) for $Ra = 10^5$ and $Ha = 100$.

two cylinders where the electric current flows. In particular, it seems that at 90° the electric current in passing through the Hartmann layer of the internal cylinder makes a radial circuit with the opposite electric current in passing through the Hartmann layer of the external cylinder. The electric current follows the same path also at 270°.

Some of the heat transfer characteristics of the turbulent flow and the effect of the magnetic field are illustrated in Fig. 11 in terms of the instantaneous local Nusselt number distribution on each cylinder for $Ra = 10^5$ and $Ha = 0$ and 100. For the hydrodynamic case, there are no systematic features observed, like structures repeated in $\theta$, except of the very low heat transfer of the upper two-thirds of the cylinders (for $z > 1$) and the intense heat transfer at their lower part. Exactly the opposite heat transfer distribution (but more uniform at the upper domain) appears on the inner cylinder. In contrast, for the MHD case of $Ha = 100$ presented in Fig. 11, the uniformity of both boundaries is disturbed by local azimuthal maxima (at $\theta = 90°$ and 270°) and the additional azimuthal waves close to the regions of lower heat transfer.

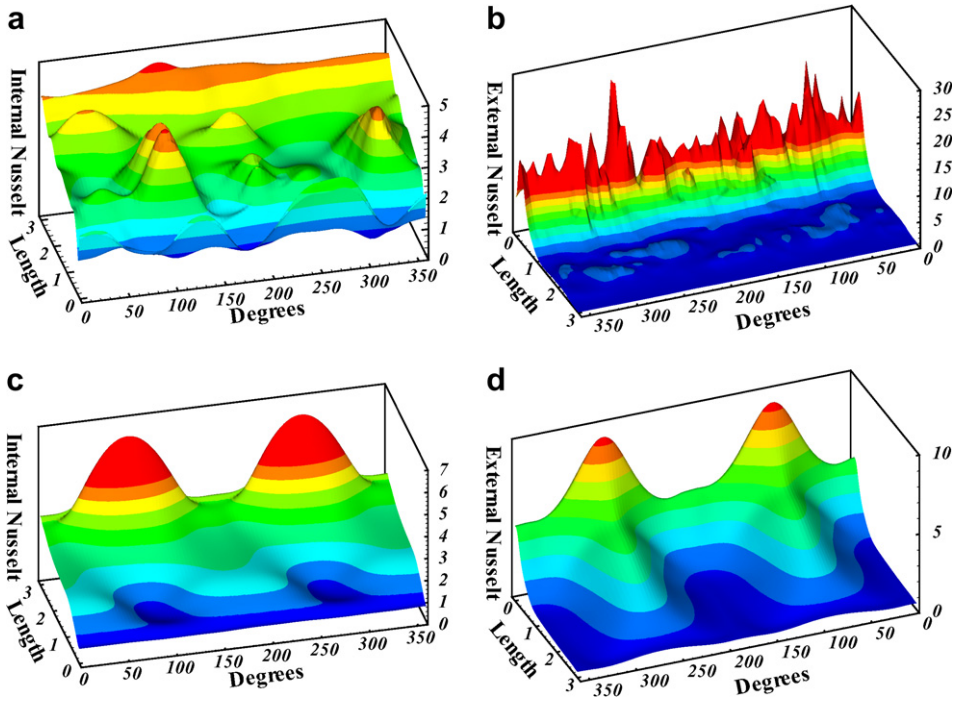


Fig. 11. Instantaneous local *Nu* distribution on the internal (left) and external (right) cylinders for $Ra = 10^5$: $Ha = 0$ (upper) and $Ha = 100$ (lower).

## 4. Conclusions

Some of the basic features of the hydrodynamic and magnetohydrodynamic, laminar and turbulent natural convection flow between two vertical concentric cylinders were studied. The results show that the increase of Rayleigh number promotes turbulence in the flow and enhances heat transfer. Interesting new results are obtained in the presence of the magnetic field. The turbulence suppression, due to the increase of the magnetic field, and its effect on the heat transfer characteristics were determined. The initially fully turbulent flow and temperature fields for small values of *Ha*, acquire quasi-periodic features with increasing magnetic field, while for large enough values of *Ha* even laminar flow appears. The presence of a strong magnetic field results in the formation of wakes parallel to its direction, in the regions close to the walls of the internal and external cylinders. Thus, in all cases studied here, the increase of the magnetic field results in the domination of conduction over convective heat transfer.

Although expensive, 3D direct numerical simulations are useful in determining accurately the features of the turbulent regime and the transitional flow when the magnetic field increases. In addition to the 3D nature of turbulence, the magnetic field has the tendency to form narrow Hartmann layers that can be a function of the azimuthal angle. Thus, 3D jets and wakes are inherent to these MHD flows, producing asymmetries even in the laminar regime. However, these are the expected working conditions of the liquid metal fusion blanket, which has been the motivating application of the present work.

## Acknowledgements

This work was performed during a mobility stay of the leading author (S.C.K.) at ULB under the cooperation of the Belgian State and Hellenic Republic Associations of EURATOM. IES was supported by an intra-European EURATOM fellowship (Contract No. 016818). The content of this paper is the sole responsibility of its authors and it does not necessarily represent the views of the Commission or its services.

## References

[1] Sarris IE, Kakarantzas SC, Grecos AP, Vlachos NS. MHD natural convection in a laterally and volumetrically heated square cavity. Int J Heat Mass Transfer 2005;48:3443–53.
[2] Li FC, Kunugi T, Serizawa A. MHD effect on flow structures and heat transfer characteristics of liquid metal – gas annular flow in a vertical pipe. Int J Heat Mass Transfer 2005;48:2571–81.
[3] Serizawa A, Ida T, Takahashi O, Michiyoshi I. MHD effect of NaK–nitrogen two phase flow and heat transfer in a vertical round tube. Int J Multiphas Flow 1990;16:761–88.
[4] Uda N, Hayase M, Chikaoka T, Inoue S, Horiike H, Miyazaki K. Natural convective heat transfer of lithium under magnetic field. Fus Eng Des 2000;51–52:893–8.
[5] Sarris IE, Zikos GK, Grecos AP, Vlachos NS. On the limits of validity of the low magnetic Reynolds number approximation in MHD natural convection heat transfer. Numer Heat Transfer – Part B 2006;50:157–80.
[6] Verzicco R, Orlandi P. A finite-difference scheme for three-dimensional incompressible flow in cylindrical coordinates. J Comput Phys 1996;123:402–14.
[7] Sarris IE, Dritselis CD, Grecos AP, Vlachos NS. Direct numerical simulation of MHD natural convection cooling in a vertical

cylindrical container. In: 1st national conference of mechanical and electrical engineering, Athens, Greece; 2005.
[8] De Vahl Davis G, Thomas RW. Natural convection between concentric vertical cylinders. Phys Fluids 1969 (Suppl. 2): 198–207.
[9] Grötzbach G. Spatial resolution requirements for direct numerical simulation of the Rayleigh–Bernard convection. J Comput Phys 1983;49:241–64.
[10] Aurnou JM, Olson PL. Experiments on Rayleigh–Bernard convection, magnetoconvection and rotating magnetoconvection in liquid gallium. J Fluid Mech 2001;430:283–307.
[11] Burr U, Müller U. Rayleigh–Bénard convection in liquid metal layers under the influence of a horizontal magnetic field. J Fluid Mech 2002;453:345–69.
[12] Todd L. Hartmann flow in an annular channel. J Fluid Mech 1967;28:371–84.